The Astrophysical Journal, 582:945–953, 2003 January 10
© 2003. The American Astronomical Society. All rights reserved. Printed in U.S.A.

X-RAY EMISSION FROM THE JETS OF XTE J1550−564

P. Kaaret,[1] S. Corbel,[2] J. A. Tomsick,[3] R. Fender,[4] J. M. Miller,[5,6] J. A. Orosz,[7] A. K. Tzioumis,[8] and R. Wijnands[5,6]

Received 2002 June 14; accepted 2002 September 3

ABSTRACT

We report on X-ray observations of the large-scale jets recently discovered in the radio and detected in X-rays from the black hole candidate X-ray transient and microquasar XTE J1550−564. On 2002 March 11, X-ray emission was detected 23″ to the west of the black hole candidate and was extended along the jet axis with an FWHM of 1″.2 and a full width at 10% of maximum intensity of 5″. The morphology of the X-ray emission matched well to that of the radio emission at the same epoch. The jet moved by 0″.52 ± 0″.13 between 2002 March 11 and June 19. The apparent speed during that interval was 5.2 ± 1.3 mas day^{-1}. This is significantly less than the average apparent speed of 18.1 ± 0.4 mas day^{-1} from 1998 to 2002, assuming that the jet was ejected in 1998 September, and indicates that the jet has decelerated. The X-ray spectrum is adequately described by a power law with a photon index near 1.8 subject to interstellar absorption. The unabsorbed X-ray flux was 3.4×10^{-13} ergs cm^{-2} s^{-1} in the 0.3–8 keV band in 2002 March and decreased to 2.9×10^{-13} ergs cm^{-2} s^{-1} in June. We also detect X-rays from the eastern jet in 2002 March and show that it has decelerated and dimmed since the previous detections in 2000.

Subject headings: black hole physics — stars: individual (XTE J1550−564) — stars: winds, outflows — X-rays: binaries

1. INTRODUCTION

Jets are a ubiquitous facet of accretion in systems ranging from young stellar objects, to Galactic X-ray binaries, to active galactic nuclei (AGNs). Many important questions regarding jet formation and propagation remain unanswered, and new data will likely be required to resolve them. Observations of systems within the Galaxy hold the great advantage that their evolution is rapid. Processes requiring millions of years in AGNs can unfold in a few years for stellar mass scale systems, so that the dynamics can be studied directly.

Corbel, Fender, & Tzioumis (2002a) and Corbel et al. (2002b) recently discovered a large-scale, relativistic radio and X-ray–emitting jet from the X-ray transient XTE J1550−564. The source is a Galactic black hole candidate, and the mass of the compact object is constrained to be 8–12 $M_\odot$ (Orosz et al. 2002). A superluminal jet ejection event had been previously observed from this source in the radio in 1998 September (Hannikainen et al. 2001) during a very bright X-ray outburst (Sobczak et al. 1999). Detection of the large-scale radio jet to the west of XTE J1550−564 led to a reanalysis of archival *Chandra* data and discovery of an X-ray jet to the east of XTE J1550−564 (Corbel et al. 2002b; Tomsick et al. 2002). This X-ray jet exhibits proper motion directly away from XTE J1550−564. Based on the angular separations and the measured proper motion, the most likely epoch of origin of these large-scale jets is near the major X-ray outburst that peaked on 1998 September 20 (Sobczak et al. 1999), and we adopt this date as the origin of the currently observed jets (Corbel et al. 2002b).

Discovery of the large-scale radio jet also led to new observations of XTE J1550−564 made with the *Chandra X-Ray Observatory* (Weisskopf et al. 2002), which are described here. The subarcsecond resolution of *Chandra* delivered by the High-Resolution Mirror Assembly (van Speybroeck et al. 1997) has allowed us to detect and resolve X-ray emission from the western jet. In addition, we have again detected the eastern jet. In the following, § 2 presents the new observation and source detections, § 3 contains our results on the spectrum, morphology, motion, and variability of the eastern jet, § 4 describes our new data on the western jet, and § 5 includes a few comments on the implications of these results.

[1] Harvard-Smithsonian Center for Astrophysics, 60 Garden Street, Cambridge, MA 02138; pkaaret@cfa.harvard.edu.
[2] Université Paris VII and Service d'Astrophysique, Centre d'Etudes de Saclay, F-91191 Gif-sur-Yvette, France.
[3] Center for Astrophysics and Space Sciences, Code 0424, University of California at San Diego, La Jolla, CA 92093-0424.
[4] Astronomical Institute "Anton Pannekoek," University of Amsterdam and Center for High Energy Astrophysics, Kruislaan 403, 1098 SJ Amsterdam, Netherlands.
[5] Center for Space Research, Massachusetts Institute of Technology, 77 Massachusetts Avenue, Cambridge, MA 02139.
[6] Chandra Fellow.
[7] Astronomical Institute, Utrecht University, Postbus 80000, 3508 TA Utrecht, Netherlands.
[8] Australia Telescope National Facility, Commonwealth Science and Industrial Research Organisation, P.O. Box 76, Epping, NSW 1710, Australia.

2. OBSERVATIONS AND SOURCE DETECTION

XTE J1550−564 was observed on 2002 March 11 and June 19 with the *Chandra X-Ray Observatory* (Weisskopf et al. 2002) using the Advanced CCD Imaging Spectrometer spectroscopy array (ACIS-S; Bautz et al. 1998) using Director's Discretionary Time in response to a Target of Opportunity request based on the discovery of the western radio jet (Corbel et al. 2002a) and a follow-up request made after discovery of X-ray emission from the western jet. For the March observation (observation ID [ObsID] 3448), a total of 26,118 s of useful exposure were obtained with the ACIS-S operated in a 1/4 subarray mode with only the S3 chip read out to minimize pileup

for XTE J1550−564, which was in the decay phase of a recent X-ray outburst and expected to be relatively bright during the observation. The roll angle of 68° placed the short axis of the field of view in the subarray mode nearly along the jet axis, but the useful field of view along that axis, ∼120″, was still adequate to image both jets. For the June observation (ObsID 3672), a total exposure of 18,025 s was obtained with the ACIS-S operated in the full array mode with six ACIS chips read out.

The data were subjected to the standard data processing (ASCDS v6.6.0 using CALDB v2.12), and then customary event processing and filtering procedures, from the Chandra Interactive Analysis of Observations (CIAO) software package v2.2.1, were applied to produce a level 2 event list. Light curves including all valid events on the S3 chip were constructed to search for times of high background. In both observations, the count rate appears uniform with no obvious flares.

Images of the region around XTE J1550−564 extended 120″ along the jet axis and 60″ perpendicular to the jet axis were constructed using photons in the energy band 0.3–7 keV. We searched for sources using *wavdetect* (Freeman et al. 2002), the wavelet-based source detection routine in CIAO. Four sources were detected at significances greater than 4 σ. One source is coincident with XTE J1550−564, and two others lie along the jet axis. The western jet was detected in both March and June, while the eastern jet was detected only in March. The fourth source, at R.A. = $15^h50^m53^s.05$, decl. = $-56°29'02''.0$ (J2000.0), does not lie along the jet axis and is identified with a relatively nearby K/M dwarf present in optical images of the field. A portion of the March image along the jet axis and containing XTE J1550−564 and its two jets is shown in Figure 1.

We adjusted the astrometry of each image so that the position of the source coincident with XTE J1550−564 matches the accurately measured radio position. A shift of 0″.76 was required for the March observation and a shift of 0″.22 for June. Both shifts are within the absolute astrometric accuracy of *Chandra*. The statistical error on the source positions is less than 0″.22 (1 σ) in all cases and less than 0″.1 for XTE J1550−564. However, care must be taken in comparing positions of the jet sources due to their finite extent as discussed below.

We defined source regions using ellipses with radii 4 times the radius of 50% encircled energy calculated from the observed photons for each source by *wavdetect*. The diameter of the ellipse for XTE J1550−564 is 3″.9, which is consistent with that expected for an on-axis point source (8 times the ∼0″.5 half-power radius for ACIS-I). We extracted counts for each source region and a corresponding background region. The exposure was calculated for a monochromatic beam of 1.5 keV. The exposure over the regions including XTE J1550−564 and the western jet is uniform to within 2%. The region including the eastern jet lies over a CCD node boundary, and the exposure is up to 15% lower. We translated the count rates to photon fluxes using the exposure, then to energy fluxes in the 0.3–7 keV band assuming a power-law spectrum with a photon index of 1.8 and a column density equal to the total Galactic column in the direction of XTE J1550−564, which we take to be $N_H = 9.0 \times 10^{21}$ cm^{-2} based on radio measurements of the H I column density (Dickey & Lockman 1990) along the line of sight. This N_H value is consistent with the one measured by high-resolution X-ray spectroscopy of XTE J1550−564 by Miller et al. (2002). The properties of the three sources along the jet axis are listed in Table 1.

Below, we also include results from archival *Chandra* data. Observations with two-dimensional imaging are available for 2000 June 9, August 21, and September 11. These data and the analysis of the eastern jet are described in Tomsick et al. (2002). Each observation is brief with an exposure of no more than 5200 s. The 2000 June observation had a grating in place, while the others did not.

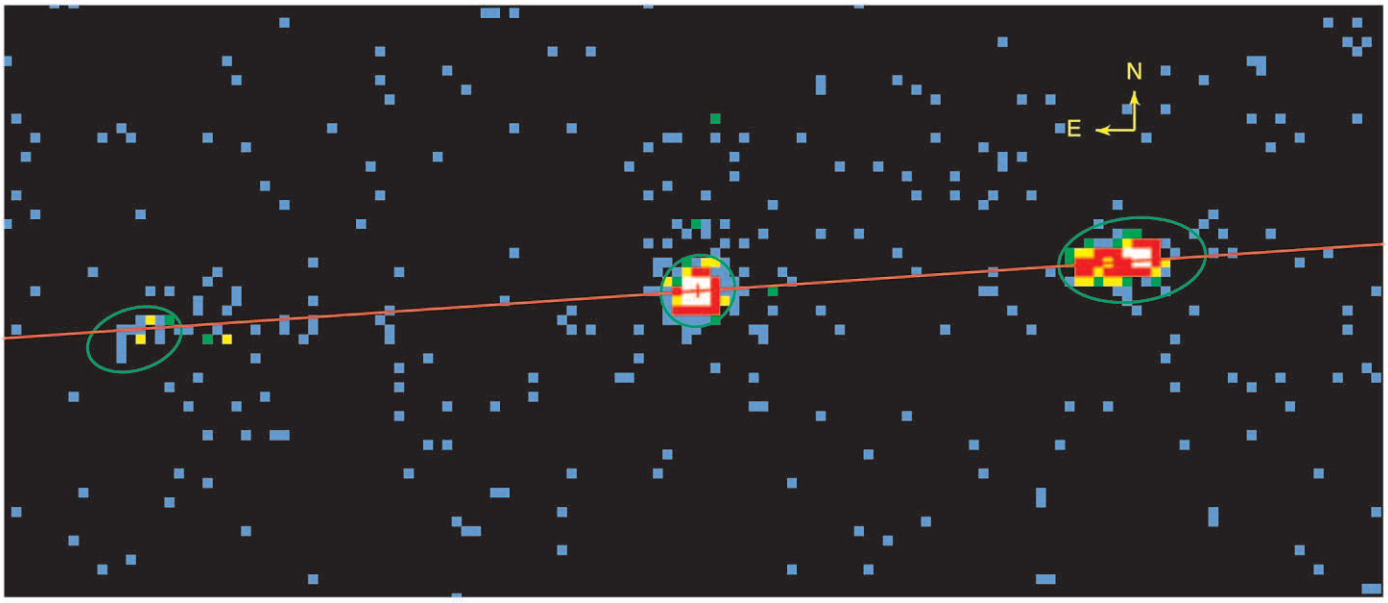

FIG. 1.—X-ray image of XTE J1550−564 for the 0.3–7 keV band taken on 2002 March 11. The color of each pixel represents the number of X-ray counts: black = 0 counts, blue = 1, green = 2, yellow = 3–4, red = 5–20, white = 21–330. The green ellipses are source regions and indicate detection of the western and eastern jets in addition to XTE J1550−564 itself. The red line is the axis of the superluminal jet emission at a position angle of −86°.1 (D. Hannikainen 2002, private communication). The arrows indicating north and east are 2″ long.

TABLE 1
X-Ray Sources near XTE J1550−564

Date (1)	R.A. (2)	Decl. (3)	S/N (4)	Counts (5)	Flux (6)	Comments (7)
March	15 50 58.66	−56 28 35.2	334.3	1163.4	4.64	XTE J1550−564
June	15 50 58.66	−56 28 35.2	26.3	54.5	0.31	
March	15 50 55.97	−56 28 33.6	122.5	409.1	1.64	Western jet
June	15 50 55.90	−56 28 33.6	87.4	238.2	1.36	
March	15 51 02.16	−56 28 37.7	4.9	18.4	0.08	Eastern jet
June	...	...	...	...	...	Not detected

Note.—Units of right ascension are hours, minutes, and seconds, and units of declination are degrees, arcminutes, and arcseconds. Col. (1): Date of observation. Cols. (2) and (3): Position of the source in J2000.0 coordinates. Col. (4): Significance of the source detection as calculated by *wavdetect*. Col. (5): Net counts in the 0.3–7 keV band. Col. (6): Observed (absorbed) source flux in units of 10^{-13} ergs cm^{-2} s^{-1} in the 0.3–7 keV band calculated assuming a power-law spectrum with photon index of 1.8 and Galactic absorption. Col. (7): Comments on the sources. There are two rows for each source: one for the March observation and one for the June observation.

3. WESTERN JET

3.1. *Spectrum*

We extracted a spectrum for the western jet from the March observation using CIAO tools and applied the recent correction for the low-energy quantum efficiency degradation of the ACIS. We fitted the spectrum using XSPEC (see Fig. 2). The spectrum is adequately fitted with a power-law model with absorption by material with solar abundances. With the equivalent hydrogen absorption column density fixed to $N_{\rm H} = 9.0 \times 10^{21}$ cm^{-2}, the best-fit photon index is $\Gamma = 1.77$ and the allowed range at 90% confidence is 1.61–1.93 ($\Delta\chi^2 = 2.7$ for one parameter). The absorbed flux is $(1.9 \pm 0.1) \times 10^{-13}$ ergs cm^{-2} s^{-1} in the 0.3–8 keV band, and unabsorbed flux would then be 3.4×10^{-13} ergs cm^{-2} s^{-1} in the same band.

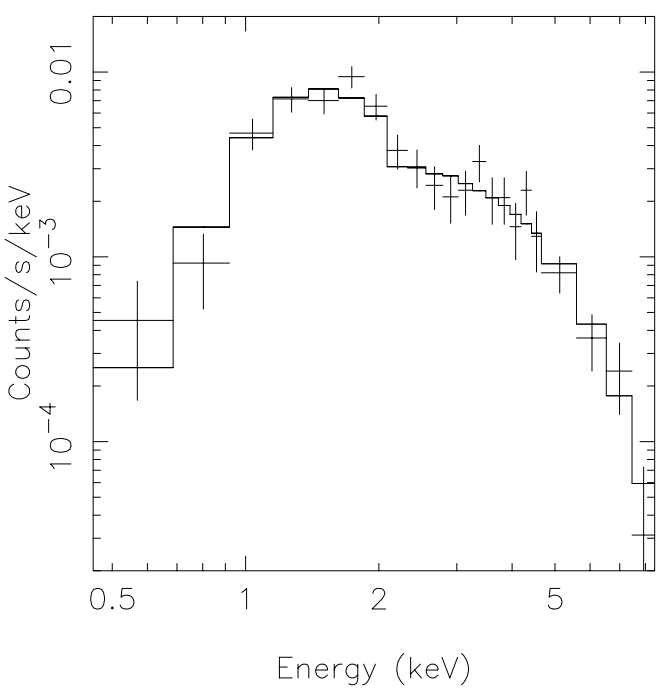

Fig. 2.—X-ray spectrum of emission from the western jet in the March observation. The curve is the best-fit power-law model with absorption fixed to the Galactic value.

Allowing the absorption column density to vary leads to an allowed range of $N_{\rm H} = (7.9\text{–}14.7) \times 10^{21}$ cm^{-2} at 90% confidence ($\Delta\chi^2 = 4.6$ for two parameters) and a corresponding range of 1.58–2.37 for the photon index. The best-fit values are $N_{\rm H} = 10.9 \times 10^{21}$ cm^{-2} and $\Gamma = 2.00$. The allowed $N_{\rm H}$ range includes the Galactic H I value. We cannot exclude extra absorption using the X-ray data.

For the June observation, the spectrum is, again, adequately fitted with a power-law model with absorption. With $N_{\rm H} = 9.0 \times 10^{21}$ cm^{-2}, the best-fit photon index is $\Gamma = 1.77$ and the allowed range at 90% confidence is 1.52–2.02. The spectrum in June appears consistent with that measured in March. The absorbed flux is $(1.6 \pm 0.1) \times 10^{-13}$ ergs cm^{-2} s^{-1} in the 0.3–8 keV band, and the unabsorbed flux is 2.9×10^{-13} ergs cm^{-2} s^{-1} in the same band.

Since there is no evidence of spectral variability, we fitted the two data sets simultaneously to obtain better constraints on the fit parameters. With $N_{\rm H} = 9.0 \times 10^{21}$ cm^{-2}, the best-fit photon index is $\Gamma = 1.77$ and the allowed range at 90% confidence is 1.64–1.90. Allowing the absorption column density to vary leads to $N_{\rm H} = (9.9^{+2.9}_{-2.2}) \times 10^{21}$ cm^{-2} and $\Gamma = 1.87 \pm 0.31$ at 90% confidence ($\Delta\chi^2 = 4.6$ for two parameters).

In addition to the nonthermal power-law model, we also fitted the combined data with the MEKAL model, which is appropriate for thermal emission from hot diffuse gas. With $N_{\rm H}$ fixed to the Galactic value, an adequate fit was obtained with $kT = 5.6^{+2.2}_{-1.1}$ keV. A simple thermal bremsstrahlung model gives a similar temperature range, $kT = 6.1^{+2.5}_{-1.5}$ keV. No prominent line emission is observed. However, the limits on the equivalent width are not strongly constraining (varying from 100 eV to 1.3 keV at 90% confidence [$\Delta\chi^2 = 2.7$] for a narrow line with energy in the range 3–7 keV).

3.2. *Morphology and Motion*

The X-ray counterpart of the western jet appears extended. Figure 3 shows the X-ray images from both *Chandra* observations with radio contours obtained from observations made on 2002 January 29 using the Australian Telescope Compact Array (ATCA; Corbel et al. 2002b) superimposed on the 2002 March 11 *Chandra* data. The ATCA image of the compact source XTE J1550−564 appears extended along a northwest-southeast axis as a result of partial synthesis caused by the limited parallactic

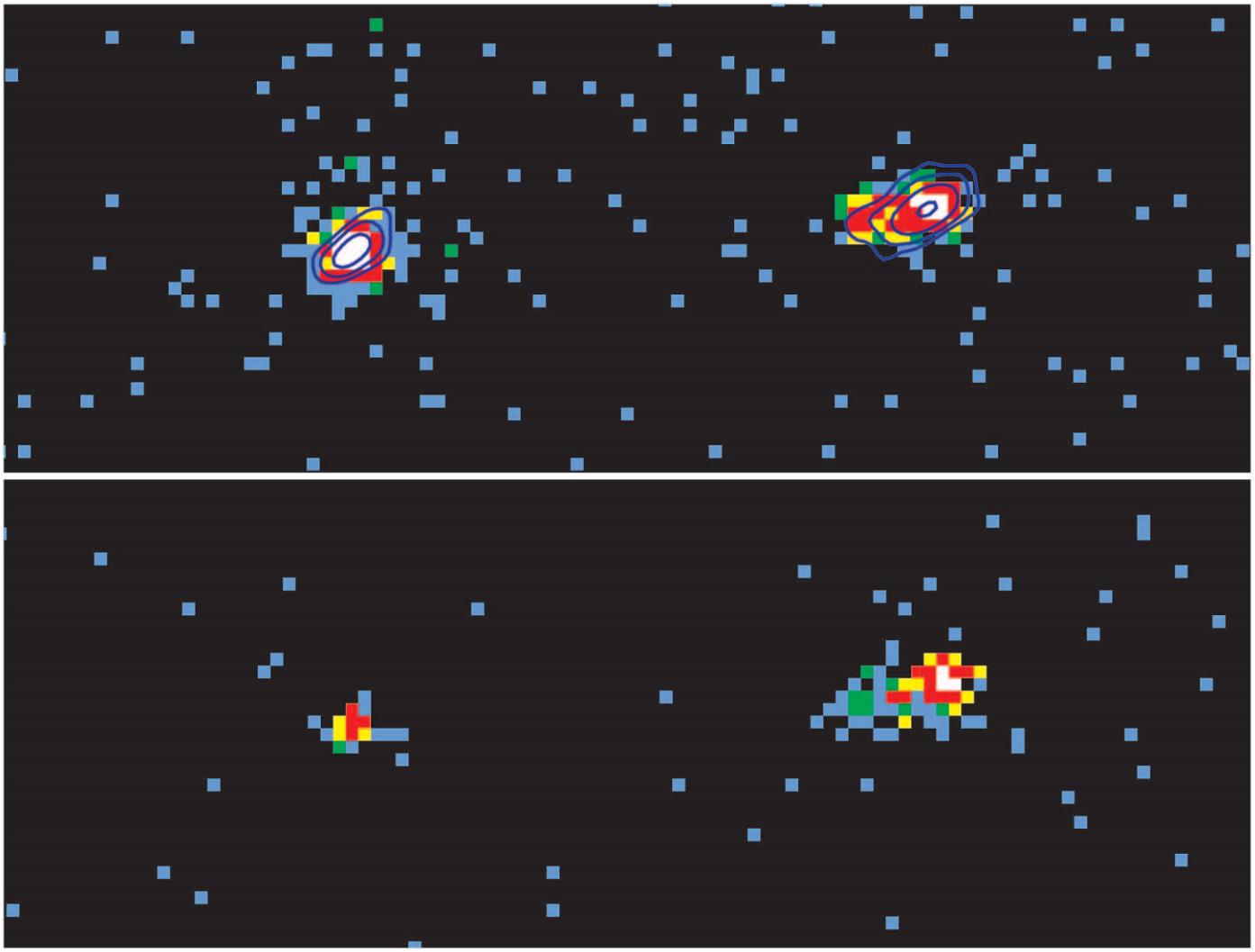

FIG. 3.—X-ray images of XTE J1550−564 (on the left) and the western jet (on the right). The top panel is from the 2002 March 11 observation, and the bottom panel is from the 2002 June 19 observation. The X-ray data are for the 0.3–7 keV band, and the color scale and orientation are the same as in Fig. 1. The top panel has radio contours (*dark blue curves*) from an observation on 2002 January 29 superimposed. The contour levels are 0.2, 0.4, 0.8, and 1.6 mJy.

angle coverage with the linear ATCA array. However, in addition to the extent caused by partial synthesis, there is a true, physical extent to the western radio jet. The peak of the jet emission is toward the west (away from XTE J1550−564), and there is lower intensity emission extending to the east, back toward XTE J1550−564. The morphology of the X-ray source closely matches that of the radio source.

We define the jet axis using the positions of the X-ray sources corresponding to XTE J1550−564 and the western jet, as reported in Table 1. The resulting position angle is $-85\overset{\circ}{.}9 \pm 1\overset{\circ}{.}3$, in good agreement with the position angle of $-86\overset{\circ}{.}1 \pm 0\overset{\circ}{.}8$ reported for the superluminal jets (D. Hannikainen 2002, private communication) and with the position angle of $-85\overset{\circ}{.}8 \pm 1\overset{\circ}{.}0$ reported for the radio western jet (Corbel et al. 2002b). To determine if the jet tails lie along the jet axis, we calculated the average azimuthal angle for events between 2″ and 6″ from the western jet position and within ±40° in azimuth of a vector pointing back to XTE J1550−564. The average azimuthal angle is $2\overset{\circ}{.}2 \pm 1\overset{\circ}{.}9$ for the March data and $7\overset{\circ}{.}4 \pm 3\overset{\circ}{.}2$ for the June data. The tail of the western jet appears aligned with the jet axis in the March data but may be slightly skewed to the south in the June data. However, the skew is only marginally statistically significant and may be affected by uncertainty in the true position of the jet peak, discussed below.

To study the morphology and motion of the X-ray jet, we decomposed the image along axes parallel and perpendicular to the jet axis (as defined above). We calculated the displacement of each X-ray event parallel and perpendicular to this axis. Figure 4 shows the profile of X-ray counts along the jet axis from the two observations. All photons with energies in the range 0.3–7 keV and within 2″ of the jet axis in the perpendicular direction are included. In the March data, both jets are clearly present. In the June data, there is no strong source at the location of the eastern jet, but there may be some diffuse emission above the background level. The western jet appears to have moved away from XTE J1550−564.

For the March observation, the peak of the X-ray emission of the western jet is displaced by 0″.6 (along the jet axis and away from XTE J1550−564) from the position reported in Table 1, which is the centroid over the region containing 50% of the encircled energy (Freeman et al. 2002). Hence,

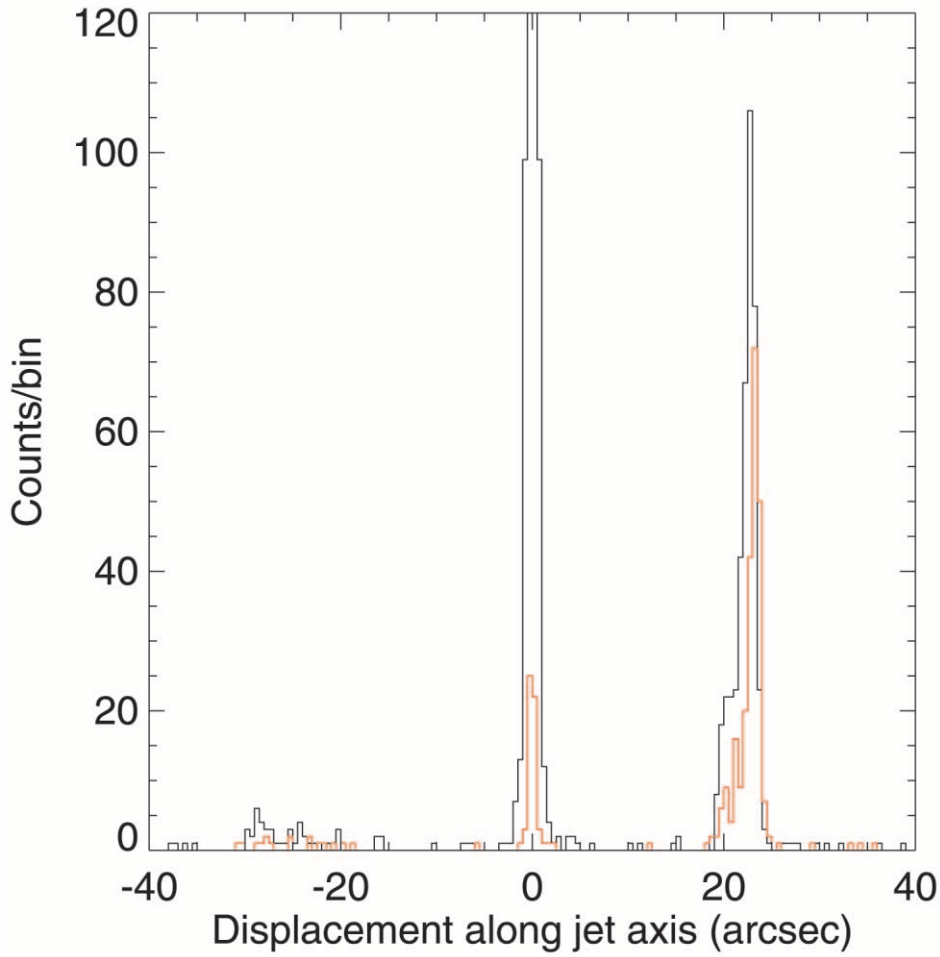

FIG. 4.—Distribution of X-ray counts along the jet axis. The black line is for the March observation, and the red line is for the June observation. The bin size is 0″.5.

caution is warranted when comparing the jet position to positions found in other observations.

To measure the relative position of the western jet in the March and June observations, we used a Kolmogorov-Smirnov (K-S) test to permit comparison of unbinned position data. We used the position along the jet axis for each event calculated above. We added an offset, in the range from −1″ to +1″, to the June event positions and then compared the offset positions with the March event positions within ±8″ of the western jet peak. The best match occurred for an offset of 0″.52. Given this offset, the K-S test gives a 61% probability that the two samples are drawn from the same parent distribution. To evaluate the uncertainty in the offset, we integrated the K-S test probability distribution as a function of offset and found the offsets corresponding to 5% and 95% of the full integral (i.e., the 90% confidence interval). These are 0″.39 and 0″.60. The hypothesis that the two distributions are the same with zero offset is rejected at the level of 5×10^{-13}. The western jet moved by 0″.52 ± 0″.13 between the March and June observations.

The morphology of the western jet does not appear to have changed, even though it moved. Figure 5 shows the western jet profiles along the jet axis from the March and June observations, with the June data shifted by 0″.52 and scaled so that the peaks match. As noted above, a K-S test is consistent with the two profiles being the same.

The figure also shows the data for XTE J1550−564 itself from the March observation, rescaled and displaced to match the peak at the western jet. From its time variability, we know that the X-ray emission from XTE J1550−564 must arise from what is effectively a point source for the angular resolution of *Chandra*. Hence, we use XTE J1550−564 as a calibration of the point-spread function for the observation to determine the spatial extent of the emission from the western jet. This procedure accounts for any aspect jitter during the observation and also for any source extent induced by scattering of the X-rays in the interstellar medium (ISM) between us and the source. The spectrum of XTE J1550−564 during the March observation is quite similar to that found for the western jet, so effects due to the energy dependence of the *Chandra* point-spread function should be negligible. Both sources are sufficiently close to the aim point so that the degradation of the *Chandra* point-spread function off-axis should also be negligible.

Comparison of the rescaled profile of XTE J1550−564 with the profile of the X-ray emission from the western jet in the March observation shows that the western jet is extended. The leading edge of the X-ray source (the edge away from XTE J1550−564) is approximately consistent with the profile of a point source. The trailing edge is clearly extended. The FWHM of the source is 1″.2, and the full width at 10% of maximum intensity is 5″.

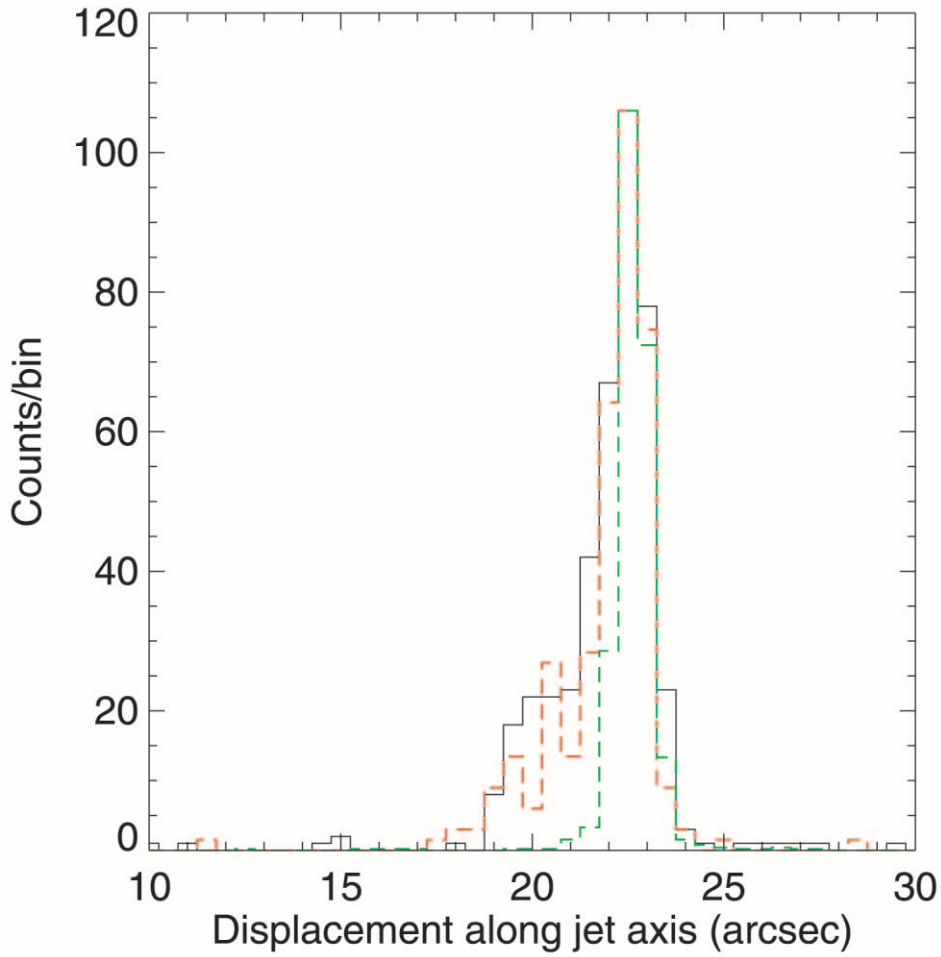

FIG. 5.—Distribution of X-ray counts in the western jet along the jet axis. The black solid line is for the March observation, the red dashed line is for the June observation, and the green dashed line is the profile of XTE J1550−564 from March. The latter two profiles have been shifted and rescaled to match the peak of the first. The bin size is 0″.5.

Figure 6 shows the distribution of X-ray counts perpendicular to the displacement axis for the western jet and XTE J1550−564 in the March data. We used X-rays with energies in the range 0.3–7 keV and with displacements along the jet axis of up to ±5″ from the respective source position as reported in Table 1. A K-S test shows that the two distributions are inconsistent at the 97% confidence level (2.2 σ). The western jet may be slightly extended perpendicular to the jet axis, but the evidence is weak. Deconvolving, assuming that the physical width adds in quadrature with the instrumental width, we place an upper limit of 0″.8 (FWHM) on the extent of the X-ray western jet perpendicular to the jet axis. The perpendicular distribution of the western jet found from the June data is consistent with that in the March data. The X-ray western jet is clearly much more extended along the jet axis than perpendicular to it.

3.3. *Variability*

To investigate the variability of the X-ray western jet, we examined archival *Chandra* data on XTE J1550−564 from 2000 June, August, and September. Using a large region extending ±4″ perpendicular to the jet axis and covering the full extent of the western jet beginning 11″ from XTE J1550−564 and extending 2″ beyond its position in 2002, we find no evidence for X-ray emission from the western jet in any of the archival observations with upper limits (2 σ) on the ACIS counting rate, which are fractions of 0.10–0.16 of the counting rate in our 2002 March data. Combining the 2000 August and September observations, in which the ACIS was not partially blocked by a grating, we find 6 counts in a total exposure of 9557 s. Given a mean of 6, the 90% confidence upper bound from a Poisson distribution is 9 counts, leading to a 90% confidence upper bound on the count rate from the western jet of 0.00094 counts s^{-1}. This is 6% of the rate in the 2002 March observation, corresponding to an upper bound on the absorbed flux (assuming identical spectral parameters) of 1.1×10^{-14} ergs cm^{-2} s^{-1} in the 0.3–8 keV band. This analysis assumes that none of the counts are due to background. Performing a background subtraction would reduce this limit.

During 2002, the flux decayed between March and June. Using the two flux measurements to calculate the $1/e$-folding time for an exponential decay, we find 327 ± 95 days. However, two data points are insufficient to determine the shape of light-curve decay.

4. EASTERN JET

The new *Chandra* observations add one additional detection to the results presented in Tomsick et al. (2002). The

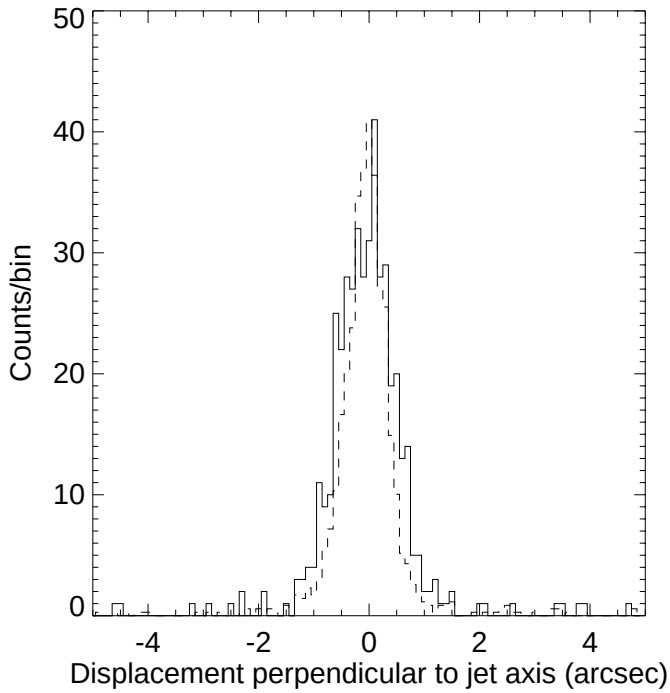

FIG. 6.—Distribution of X-ray counts perpendicular to the jet axis from the 2002 March observation. The solid line is for the western jet. The dashed line is the profile of XTE J1550−564 rescaled to match the peak of emission in the western jet. The bin size is 0″.1.

source contains far fewer counts than the western jet, and so we concentrate on the position and flux of the source.

The proper motion of the eastern jet is shown in Figure 7. The figure includes the three data points from Tomsick et al. (2002) and our new data point for 2002 March 11. Tomsick et al. (2002) showed that the apparent velocity of the eastern jet in 2000 was lower than the minimum velocity allowed during the superluminal ejection (Hannikainen et al. 2001), thus indicating that the eastern jet has decelerated. The 2002 March point is inconsistent with an extrapolation of the velocity measured from the 2000 data and indicates that this deceleration has continued.

We fitted the proper motion data with a model in which the jet has a deceleration proportional to its velocity relative to the X-ray binary (which we assume to be roughly at rest relative to the ISM). The velocity profile is then a decaying exponential, and the observed position evolution is modified by light-travel delays. Our model has three fitted parameters: the initial jet speed divided by the speed of light β_0, the timescale ($1/e$-folding time) for the velocity decay τ, and the jet angle relative to the line of sight θ. The assumed source distance affects the fitted parameters. For a source distance of 4 kpc, we find an adequate fit (shown in Fig. 7) with $\beta_0 = 0.94$, $\tau = 1030$ days, and $\theta = 62°$. For source distances larger than 5.1 kpc, the best-fit initial speed is larger than the speed of light. However, we do not consider this a constraint on the distance as the model is rather ad hoc. For a distance of 3 kpc, the best fit is $\beta_0 = 0.82$, $\tau = 960$ days, and $\theta = 50°$. Both of these fits are consistent with the lower bound on the initial jet speed from the VLBI observations (Hannikainen et al. 2001).

Figure 8 shows the time variation of the X-ray flux of the eastern jet. The first three points are from Tomsick et al. (2002). For consistency with that analysis, we found the fluxes for the 2002 March data using a circular extraction region of 4″ radius centered on the *wavdetect* position and with an annulus with an inner radius of 5″ and an outer radius of 18″ for background estimation. We used a power-law model with photon index fixed to 1.8 and an absorption column density fixed to 9×10^{21} cm^{-2} and corrected for the degradation in the low-energy quantum efficiency of the

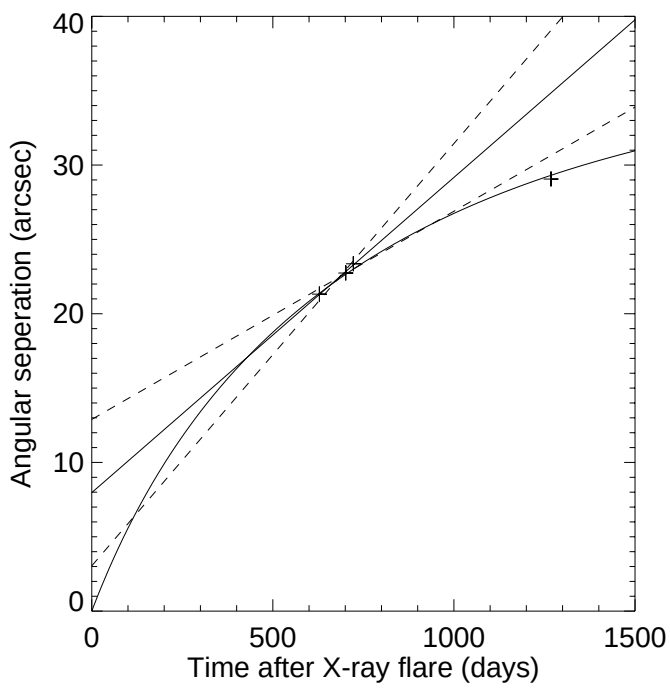

FIG. 7.—Position of the centroid of the X-ray eastern jet vs. time. The solid line is the fit to the proper motion in the 2000 data found by Tomsick et al. (2002). The dashed line indicates the uncertainty in the fit parameters. The solid curve is a decelerating jet model fit described in the text.

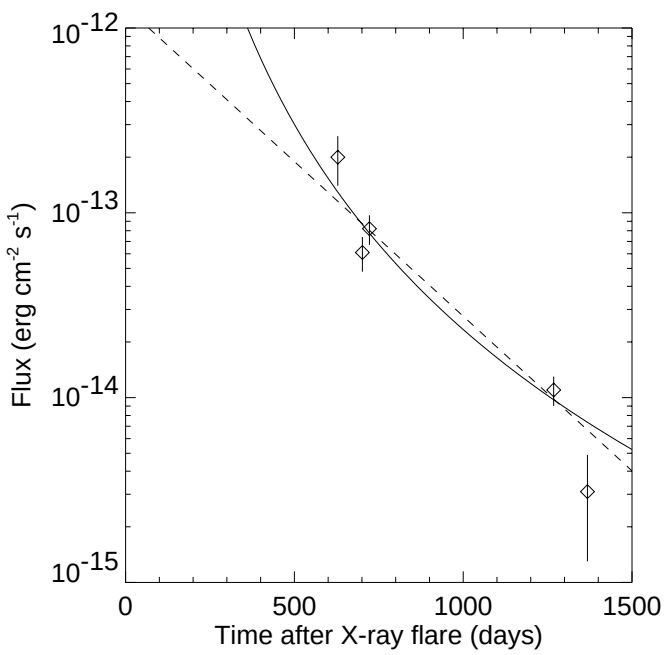

FIG. 8.—X-ray flux of the eastern jet vs. time. The curves are the power-law (*solid curve*) and exponential (*dashed curve*) decays described in the text.

ACIS. The absorbed flux in the 0.3–8 keV band was $(1.1 \pm 0.3) \times 10^{-14}$ ergs cm^{-2} s^{-1}. For June, no source was detected by *wavdetect* at the location of the western jet. We extracted counts from a circular region 4″ radius centered at the position found in March. This region is sufficiently large to include most of the diffuse emission apparent in Figure 4. With spectral parameters fixed as above, the absorbed flux in the 0.3–8 keV band is $(3 \pm 2) \times 10^{-15}$ ergs cm^{-2} s^{-1}. We interpret this number as an upper limit on the jet flux in June.

We fitted both an exponential decay and a power-law decay to the flux data. The power-law decay provides a slightly better fit, but both fits are acceptable. The index of the power-law decay is 3.7 ± 0.7. The $1/e$-folding time of the exponential decay is 260 ± 50 days. The extrapolated flux at the origin of the jet for the exponential decay would be $(1.3 \pm 0.5) \times 10^{-12}$ ergs cm^{-2} s^{-1} in the 0.3–8 keV band. This is a small fraction of the X-ray fluxes measured during the 1998 outburst. Hence, the available X-ray data are not inconsistent with an exponential decline of flux since the origin of the eastern X-ray jet.

5. DISCUSSION

The discovery of extended radio and X-ray emission from XTE J1550−564 (Corbel et al. 2002b; Tomsick et al. 2002; results reported here) represents the first detection of large-scale relativistic jets from a Galactic black hole candidate in both radio and X-rays. These large-scale jets appear to arise from a relatively brief jet injection episode (Corbel et al. 2002b) and, therefore, offer a unique opportunity to study the large-scale evolution of an impulsive jet event.

In the following, we assume that both jets were created in a single injection episode in 1998 September. The assumption is motivated by the detection of superluminal jets (Hannikainen et al. 2001) following an extremely large X-ray flare in 1998 September and the absence of any other X-ray flare of similar magnitude in continual X-ray monitoring from 1996 to 2002 (Corbel et al. 2002b). The eastern jet appears to be the approaching jet based on its larger current separation from XTE J1550−564 (Corbel et al. 2002b). The distance to XTE J1550−564 is constrained from optical observations to be in the range 2.8–7.6 kpc with a favored value of 5.3 kpc (Orosz et al. 2002).

We detected X-ray emission from the western jet on 2002 March 11 (MJD 52,344) at a separation of 23″ from the black hole candidate, implying a projected physical separation of 0.59 pc$(d/5.3$ kpc$) = 1.8 \times 10^{18}$ cm$(d/5.3$ kpc$)$ and a mean projected speed of 18.1 ± 0.4 mas day^{-1} or $0.55c(d/5.3$ kpc$)$. From the motion of the jet between March 11 and June 19, we calculate an average speed at that epoch of 5.2 ± 1.3 mas day^{-1} or $(0.16 \pm 0.04)c(d/5.3$ kpc$)$. This is significantly less than the average speed from 1998 to 2002 and indicates that the jet has decelerated. Our detection of motion in the western jet argues against it having reached a termination. The jet appears to have a relativistic bulk velocity.

The angular size of the X-ray emission perpendicular to the jet axis in the western jet is quite small, less than 0″.8 (FWHM), placing an upper bound on the jet half opening angle of 1°.0. The opening angle is small, similar to the half opening angles of Fanaroff-Riley class II (FR II; Fanaroff & Riley 1974) sources, which are less than 3° (Muxlow & Garrington 1991). The angular size of the western X-ray jet perpendicular to the jet axis limits the expansion velocity to less than $0.01c(d/5.3$ kpc$)$. At the same epoch, the eastern jet has a projected physical separation of 0.75 pc$(d/5.3$ kpc$)$.

For comparison with the properties of the western jet, we review the properties of the eastern jet at the same angular separation. From the linear fit in Tomsick et al. (2002), we find that the eastern jet passed through a separation of 23″ on MJD $51,785 \pm 16$. Fortuitously, this is consistent with the times of the 2000 August 21 and September 11 *Chandra* observations (the separations from both of those observations are consistent with 23″). As discussed in Tomsick et al. (2002), the high proper motion of the eastern jet when at a separation of 23″ argues strongly against it having reached a termination at that point. The continued motion of the eastern jet to larger separations demonstrated here reinforces this argument. At a separation of 23″, the apparent speed of the eastern jet was 21.2 ± 7.2 mas day^{-1} and the absorbed flux was $(7.2 \pm 1.0) \times 10^{-14}$ ergs cm^{-2} s^{-1} in the 0.3–8 keV band. The western (receding) jet flux at the same separation was a factor of 2.6 ± 0.4 higher than the eastern (approaching) jet flux.

The X-ray data provide measurements of the local apparent speed at equal angular separations from the origin for the approaching and receding jets. If the jets are symmetric, in terms of their velocity profiles, then it would be possible to use relativistic kinematics (Mirabel & Rodríguez 1999) to constrain the jet true speed β, inclination to the line of sight θ, and distance d. We find that $\beta \cos\theta = 0.61 \pm 0.13$ and $d = (12.6 \pm 4.4) \tan\theta$ kpc under the assumption that the jet propagation is symmetric. This would imply that the inclination angle $\theta \leq 61°$ and the jet speed $\beta \geq 0.48$ (allowing for the uncertainty in $\beta \cos\theta$).

However, the fact that the western (receding) jet is brighter than the eastern (approaching) jet argues against symmetric jet propagation. For symmetric jet propagation, the ratio of observed flux densities measured at equal separations from the core for a twin pair of optically thin isotropically emitting jets is

$$\frac{S_a}{S_r} = \left(\frac{1 + \beta\cos\theta}{1 - \beta\cos\theta}\right)^{k-\alpha}, \qquad (1)$$

where S_a is the approaching flux density, S_r is the receding flux density, β is the jet speed divided by the speed of light, θ is the jet inclination angle, α is the spectral index of the emission defined so that $S_\nu \propto \nu^\alpha$, and k is a parameter that is 2 for a continuous jet and 3 for discrete condensations (Mirabel & Rodríguez 1999). If the exponent $k - \alpha > 0$, then the approaching jet must always be brighter than the receding jet measured at the same angular separation from the core. Given the photon index quoted above (allowing the absorption to vary) and allowing a continuous jet, the minimum allowed value for the exponent is 2.6, which is well above zero. Hence, the observed brightness ratio $S_a/S_r = 0.38 \pm 0.05$ is inconsistent with symmetric jet propagation. However, because the X-ray jet detections occurred well after the initial jet ejection, we cannot independently constrain the jet ejection, which may have been symmetric.

Large intrinsic asymmetries have been observed in the radio for the jets from the microquasar GRO J1655−40 (Hjellming & Rupen 1995). Which of the two jets was brighter differed from day to day, while the kinematics of the jet propagation appeared symmetric. Asymmetries of similar magnitude could explain the ratio of X-ray fluxes

from the jets of XTE J1550−564 if the jet inclination angle is high. In this case, the X-ray emissivity of the western jet would need to be low early on, to be consistent with the nondetection in 2000, and then increase sharply at later times, to be consistent with the flux measured in 2002. Such an X-ray emissivity profile could be produced by, e.g., internal shocks produced by a faster plasmon overtaking a slower one. This would require reacceleration of particles in the jet long after its initial ejection.

Alternatively, the emission from the jets could be produced by shocks arising from interactions of the jets with the ISM. The jets appear to be moving with speeds much greater than the sound speed of the ISM. In this case, the supersonic motion of the jet should produce a shock wave. The shock will be strongest at the head of the jet and weaken around the sides of the jet (De Young 2002). This morphology matches that observed for the eastern jet. In this case, the asymmetry between the two jets may reflect nonuniformity in the ISM. If the western jet is propagating into a denser medium, it would be brighter and would have decelerated more than the eastern jet. Interaction of a relativistic plasmon with the ISM appears to consistently describe all of the available data on the large-scale jets of XTE J1550−564.

Continued observation of the jets of XTE J1550−564 offers an exciting opportunity to study the dynamics of relativistic jets on timescales inaccessible for AGN jets. New, deep observations of XTE J1550−564 will allow us to study the deceleration and evolution of the morphology, flux, and spectrum of the western jet. This may help determine whether the observed jets are due to the internal interactions of relativistic plasmons or to external interactions with the ISM. A deep observation may also permit a new detection of the eastern jet, which would further constrain its deceleration and decay. Finally, continued monitoring may eventually show the termination of the jets.

We thank Harvey Tananbaum for granting the DDT observations, Joy Nichols for exceptionally rapid processing of the data, and the CXC team for successfully executing the observation. P. K. thanks Heino Falcke, Dan Harris, and David De Young for useful discussions and acknowledges partial support from NASA grant NAG5-7405 and *Chandra* grant G01-2034X. R. W. was supported by NASA through *Chandra* Postdoctoral Fellowship grant PF9-10010 awarded by CXC, which is operated by SAO for NASA under contract NAS8-39073.

REFERENCES

Bautz, M. W., et al. 1998, Proc. SPIE, 3444, 210
Corbel, S., Fender, R., & Tzioumis, A. 2002a, IAU Circ. 7795
Corbel, S., Fender, R. P., Tzioumis, T., Tomsick, J. A., Orosz, J. A., Miller, J. M., Wijnands, R., & Kaaret, P. 2002b, Science, 298, 196
De Young, D. S. 2002, The Physics of Extragalactic Radio Sources (Chicago: Univ. Chicago Press)
Dickey, J. M., & Lockman, F. J. 1990, ARA&A, 28, 215
Fanaroff, B. L., & Riley, J. M. 1974, MNRAS, 167, 31P
Freeman, P. E., Kashyap, V., Rosner, R., & Lamb, D. Q. 2002, ApJS, 138, 185
Hannikainen, D., Campbell-Wilson, D., Hunstead, R., McIntyre, V., Lovell, J., Reynolds, J., Tzioumis, T., & Wu, K. 2001, Ap&SS Supp., 276, 45
Hjellming, R. M., & Rupen, M. P. 1995, Nature, 375, 464
Miller, J. M., et al. 2002, MNRAS, in press
Mirabel, I. F., & Rodríguez, L. F. 1999, ARA&A, 37, 409
Muxlow, T. W. B., & Garrington, S. T. 1991, in Beams and Jets in Astrophysics, ed. P. A. Hughes (Cambridge: Cambridge Univ. Press), 52
Orosz, J. A., et al. 2002, ApJ, 568, 845
Sobczak, G. J., McClintock, J. E., Remillard, R. A., Levine, A. M., Morgan, E. H., Bailyn, C. D., & Orosz, J. A. 1999, ApJ, 517, L121
Tomsick, J. A., Corbel, S., Fender, R. P., Miller, J. M., Orosz, J. A., Tzioumis, T., Wijnands, R., & Kaaret, P. 2002, ApJ, 582, 933
van Speybroeck, L. P., et al. 1997, Proc. SPIE, 3113, 89
Weisskopf, M. C., Brinkman, B., Canizares, C., Garmire, G., Murray, S., & Van Speybroeck, L. P. 2002, PASP, 114, 1